Applied Surface Science 573 (2022) 151572

Contents lists available at ScienceDirect

Applied Surface Science

journal homepage: www.elsevier.com/locate/apsusc

Full Length Article

Effect of the AlAs capping layer thickness on the structure of InAs/GaAs QD

N. Ruiz-Marín [a], D.F. Reyes [a,*], L. Stanojević [b], T. Ben [a], V. Braza [a], A. Gallego-Carro [b], G. Bárcena-González [c], J.M. Ulloa [b], D. González [a]

[a] University Research Institute on Electron Microscopy & Materials, (IMEYMAT), Universidad de Cádiz, 11510 Puerto Real (Cádiz), Spain
[b] Institute for Optoelectronic Systems and Microtechnology (ISOM), Universidad Politécnica de Madrid, Ciudad Universitaria s/n, 28040 Madrid, Spain
[c] Department of Computer Science and Engineering, University of Cádiz, Spain

ARTICLE INFO

Keywords:
InAs quantum dots
AlAs capping
(S)TEM

ABSTRACT

Recently, very thin AlAs capping layers (CLs) have been proposed as a useful tool to increase the performance of InAs/GaAs quantum dot (QDs) devices. However, the structure of QDs after AlAs deposition remains poorly understood and the mechanisms to explain it are often contradictory. In this work, the structural and compositional changes of InAs QDs using different AlAs CL thicknesses have been studied by state-of-the-art STEM-related techniques. First, the heights and In contents of InAs QDs progressively increase with the CL thickness, demonstrating that the AlAs capping produces a strong shielding effect against the decomposition of QDs. However, QD populations for CL thicknesses above 5 ML split into a bimodal distribution in which smaller lenticular QDs cohabit with bigger truncated pyramids. Second, the actual Al contents around the QDs are well below the nominal design, but increasing for thicker CLs. Its distribution is initially non-uniform, tending to accumulate on the flanks of the QDs to the detriment of the apex. Only for thicknesses above 2 ML the Al contents around the QDs start to be similar to those in the regions between the QDs, behaving as a continuous film without irregularities from 5 ML onwards.

1. Introduction

Self-assembled InAs/GaAs quantum dots (QDs) grown by Stranski-Krastanov (SK) mode have been intensively investigated in many important fields due to their elevated level of optical activity and growth control, from single photon emitters for quantum information and quantum computing [1–4] to infrared light harvesting in photodetection [5,6] and photovoltaic disciplines [7–9]. However, QDs grown by SK mode have one significant disadvantage due to the formation of a so-called wetting layer (WL) that lies between QDs, since it results in a unwanted thermally electronic coupling between the QD confined states and the extended WL states [10,11]. Recently, effective decoupling of the WL from the QDs has been achieved by capping with few monolayers of AlAs after the InAs QD formation [12–14]. Thus, it has been shown that these QDs can host highly charged excitons where up to six electrons occupy the same QD [13]. Moreover, QD photovoltaic devices with suppressed WL capture have shown huge improvements of the open-circuit voltage (V_{oc}) regarding standard QD solar cells, (SCs) together with some increase in the short circuit current [15,16].

Although two decades have passed since the first reported InAs QDs covered with AlAs capping layers (CLs) [17], the changes in the structure and in the recombination mechanisms after the deposition of AlAs remain yet unclear and seem often contradictory. Thus, different mechanisms to describe structurally the system have been proposed in the bibliography in order to explain the increase of its emission wavelength and/or the enhancement of V_{oc} in QDSCs. First, Arzberger *et al.* [17], comparing different growth temperatures, suggested that InAs QDs are fully capped from the beginning where AlAs suppresses both In segregation and In–Ga intermixing at the interface between the InAs and AlAs. The homogeneity of the islands is not significantly improved but they found an inflection point in the PL properties when the thickness of the AlAs CL is around 2–3 MLs. However, this model was questioned because later studies of In segregation in AlAs/InAs interfaces reported small differences regarding GaAs/InAs ones [18,19]. A bit later, Tsatsul'nikov *et al.* [20] proposed a breakthrough model suggesting that the deposition of thin AlAs CLs results in replacement of In atoms of the WL

* Corresponding author.
E-mail addresses: nazaret.ruiz@uca.es (N. Ruiz-Marín), daniel.fernandez@uca.es (D.F. Reyes), lazar@isom.upm.es (L. Stanojević), teresa.ben@uca.es (T. Ben), veronica.braza@uca.es (V. Braza), alejandro.gallego@alumnos.upm.es (A. Gallego-Carro), guillermo.barcena@uca.es (G. Bárcena-González), jmulloa@isom.upm.es (J.M. Ulloa), david.gonzalez@uca.es (D. González).

https://doi.org/10.1016/j.apsusc.2021.151572
Received 27 June 2021; Received in revised form 16 September 2021; Accepted 8 October 2021
Available online 12 October 2021

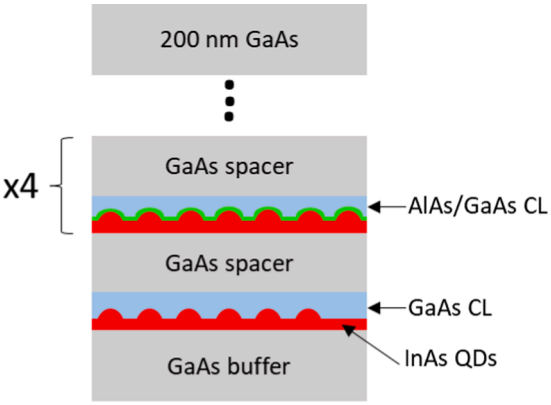

Fig. 1. Scheme of samples structure. The thickness of the AlAs CLs is 1, 2, 3 and 5 MLs for **sample A** and 2, 5, 7.5 and 10 MLs for **sample B**.

by Al ones, with a reversed migration of In atoms towards the uncapped QDs, leading to a significant height increase of these InAs QDs. Remarkably, the WL either is absent or has a smaller In content in the case of the AlAs overgrowth. Diverging from these studies, Ferdos *et al.* [21], using AFM measurements, indicated that at the beginning the decomposition of InAs QDs by using AlAs CLs is even much stronger than in the case of GaAs capping. Consequently, WL is more enriched with In at this initial stage than during GaAs capping, though in both cases the effect saturates after 3–4 nm of capping. More recently, Tutu *et al.* [15], with the aim to explain the enhancement of V_{oc} in InAs QDSCs capped by 2 ML of AlAs, compiled a mix model by collecting some ideas from previous papers. First, they pointed to the disappearance of the WL by a replacement of In atoms by Al [20]. Second, they suggested an accumulation of AlAs at the top of the QDs with a decreased stress at the edges of the QDs [22] that reduces In migration giving place to a larger QDs [17,21]. However, they do not explain where the excess of In coming from the WL is located. In addition, growth parameters such substrate temperature [17], growth rate [18], number of MLs deposited [21] or annealing treatments [23,24] have a strong influence in the properties of this system.

As has been seen, despite the renewed interest in the capping of InAs QDs by using thin AlAs layers, the descriptions of this system, based on both the degree of decomposition of WL/QDs and the degree of covering of the QDs, are very varied and contradictory. To shed some light on the topic, a complete analysis of the structural and compositional properties of InAs QDs covered by thin AlAs CLs with different thicknesses is carried out by combining different state-of-art STEM techniques. The changes in the average QD volume, composition and density, covering a statistically significant number of buried QDs are presented, as well as the covering degree for each case. As will be shown in the article, covering InAs/GaAs QD layers by thin AlAs layers has a strong impact on the structure and does not follow linear tendencies with the AlAs thickness in all the parameters.

2. Material and methods

Two samples were growth by solid source MBE on Si doped (1 0 0) n^+ GaAs substrate under As_4 stabilized conditions ($1x10^{-5}$ torr As_4 beam equivalent pressure). In both samples, 5 QD layers were grown over a 700 nm-thick *n*-GaAs base buffer by depositing 2.8 MLs of InAs at 460 °C and 0.045 ML/s. The **sample A** (see Fig. 1) consists of 5 InAs QDs layers capped by thin layers with 0, 1, 2, 3 or 5 ML of AlAs at 0.5 ML/s, respectively, plus 30 ML of GaAs, all grown at 480 °C. Before AlAs deposition, a 20 s growth interruption under As flux was performed ($8x10^{-6}$ torr As_4 beam equivalent pressure). Each QD layer is separated by 50 nm GaAs grown at 580 °C to suppress the formation of dislocations [25]. The **sample B** was grown under the same conditions with InAs QDs layers capped with 0, 2, 5, 7.5 and 10 ML of AlAs. In the following, each layer in both samples is named as **CL#**, being # the number of MLs of AlAs. Both samples were finished with a 200 nm GaAs layer grown at

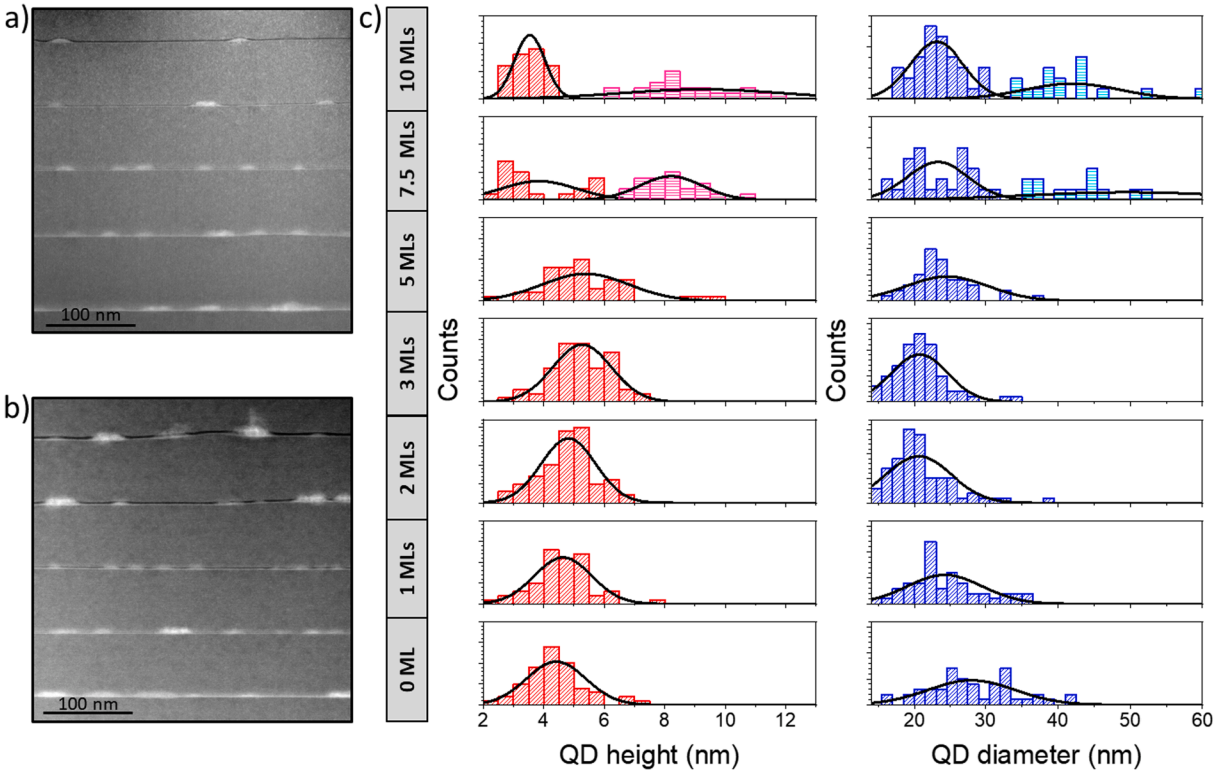

Fig. 2. Global views of sample A (a) and B (b) in LAADF conditions. Remarkably, it is the presence of plastic relaxed giant QDs in **CL7.5** and **CL10** layers. (c) Histograms of the QD height and base diameter of the different layers. Note that the size distributions are much spread from **CL5** upwards.

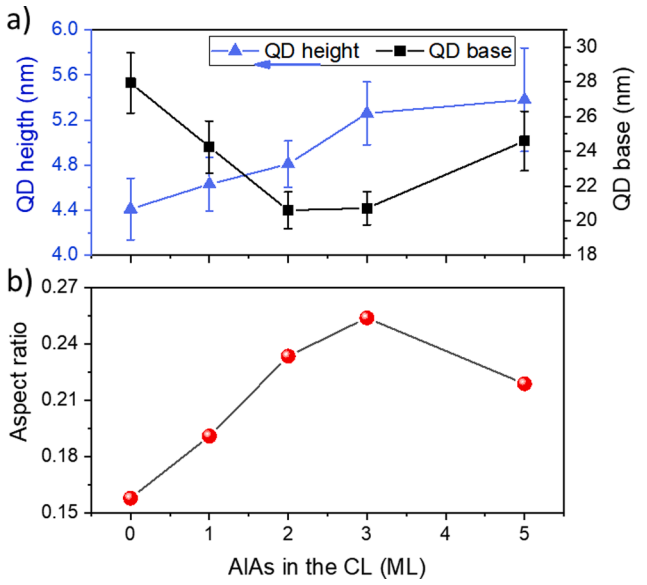

Fig. 3. (a) Average QD height and base diameter for InAs QDs layers up to 5 ML of AlAs. Errors bars are 2 times the standard error of the mean. (b) Aspect ratio versus the thickness of the AlAs CL.

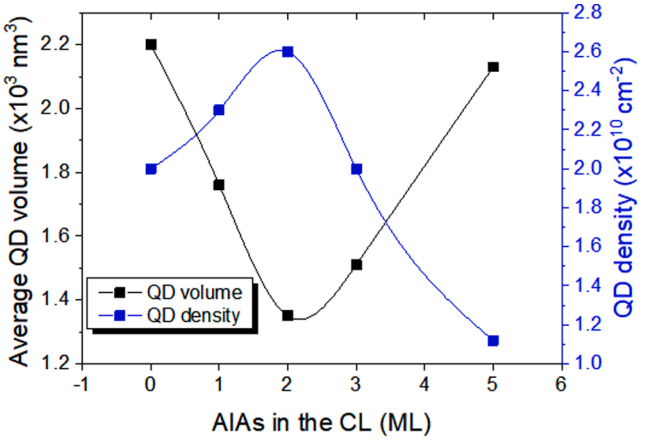

Fig. 4. Average QD volume (right) and QD density (left) versus the thickness of the AlAs CL. An inverse relationship is found between both features.

580 °C. Analyses by Low Angle Annular Dark Field (LAADF) imaging, Electron Energy Loss Spectroscopy (EELS) and Energy-dispersive X-ray spectroscopy (EDX) with ChemiSTEM® technology were performed in a double-aberration corrected FEI Titan Cubed^3 operated at 200 kV and processed using Velox® software.

3. Results

The study is divided into 3 blocks. The first one is a structural study of the morphology distribution of the population of QDs in the different layers, focusing on the changes in size, shape and superficial density. The second block deals with how the In content of the QDs is affected by the deposition of different CL thicknesses of AlAs. Finally, the last block will analyse the evolution of the Al distribution around the QD for every AlAs thickness.

3.1. Structural characterization: size, shape and QD density

In general, TEM imaging exciting the compositional sensitive g002 reflection in dark-field diffraction contrast conditions has been usually utilized to obtain the vertical and lateral dimensions of InAs/GaAs QDs [26–28]. However, the size measurement of AlAs/InAs QDs with this imaging technique is problematic, as the contrasts around the QDs change depending on both the CL content and the sample thickness, where even contrast inversions have been observed when comparing QD images of different layers. Therefore, it is difficult to measure the QD contour with accuracy using the same contrast criteria for all the layers. Looking for an alternative and using EDX mappings of the In composition for verification, we have found that the LAADF imaging technique is less sensitive to sample thickness variations than g002 for estimating the dimensions of QDs. In LAADF images with TEM sample thicknesses below 100 nm (Fig. 2.(a, b)), the regions richer in In always appear brighter than the GaAs matrix, while those richer in Al darken.

In general, the shape of most buried QDs is predominantly lenticular, which cohabit with some truncated pyramidal QDs whose percentage increases as the AlAs CL thickness does. Fig. 2.c shows histograms of the QD height, *h*, and the base diameter, *B*, for each QD layer together with their normal distribution curves. The average results for the height and diameter of the QD population of the common layers (**CL0**, **CL2** and **CL5**) of the two samples in areas of similar TEM thickness are very similar, so we have assumed that the growth conditions are reproducible and the layers are sufficiently separated to avoid influences between them. As can be seen, it can see an improvement in the distribution of the QD size parameters up to 2–3 ML of AlAs and then an exponential increase of the dispersion, where the AlAs thickest layers (**CL7.5** and **CL10** layers) present an enormous spread. All normality tests used (Chen-Shapiro, Lilliefors or Shapiro-Wilk) cannot reject normality at the level of 0.05 for the QD layers with AlAs thicknesses <5 ML, i.e. the data of these populations were significantly drawn from a normally distributed population. In the case of the thickest CLs (**CL7.5** and **CL10** layers), their QD populations are progressively split in a bimodal type distribution. Small lenticular-shaped QDs coexist together with giant truncated pyramids with base diameters of dozens of nanometres, sometimes plastically relaxed as it can be seen in Fig. 2.b. The generation of these bigger QDs deprives In amount in the surroundings giving place to regions with smaller QDs and lower superficial densities. For all these reasons, the use of AlAs CLs with thickness above 5 MLs has to be discarded in the design of MQD structures. In the following, attention will be given only to the InAs QDs layers with CL thickness up to 5 ML of AlAs.

Figure 3.a shows the average data of height and base diameters in relation to the CL thickness of AlAs. Certainly, it can be observed a continuous increase of QD heights with a small step in the case of 2–3 MLs. Nevertheless, the base diameter does not follow a linear trend, decreasing at the beginning and slightly increases thereafter. Related to this, Fig. 3.b displays the evolution of the aspect ratio defined as $r = h/B$ versus the AlAs CL thickness. The aspect ratio is a parameter widely used as a descriptor of QD shapes, since it is one of the critical factors determining QD strain, piezoelectric fields and fine structure splitting [29,30]. As can be seen, the aspect ratio follows a considerable increase from 0.15 to 0.23 with the CL thickness, reaching a maximum at 3 ML. The data distribution of the aspect ratio for the **CL7.5** and **CL10** layers (not shown here) clearly defines a bimodal population with mean values around 0.16 and 0.23. In addition, to check how it affects to the global size, QD volumes calculated assuming a spherical-dome shape are shown in Fig. 4. QD volume follows the same tendency as the QD base diameter, with a decrease from 0 to 2 ML of AlAs and an increase from 2 to 5 ML. The trend of the average QD volume is mainly controlled by the evolution of the QD base diameters rather than the changes of the height. In any case, all these outcomes point to a change in the behaviour of the QD shape when AlAs deposition is around 2–3 ML [17].

Let us now focus on the QD densities. Changes in the capped QD densities regarding the original unburied QD distributions can occur by modifying the capping growth conditions, such as their chemical nature [22,31], growth interruptions [32,33], growth rate [34,35] or growth temperature [36]. Very recently, it has been found an inverse relationship between the QD average volume and superficial QD density

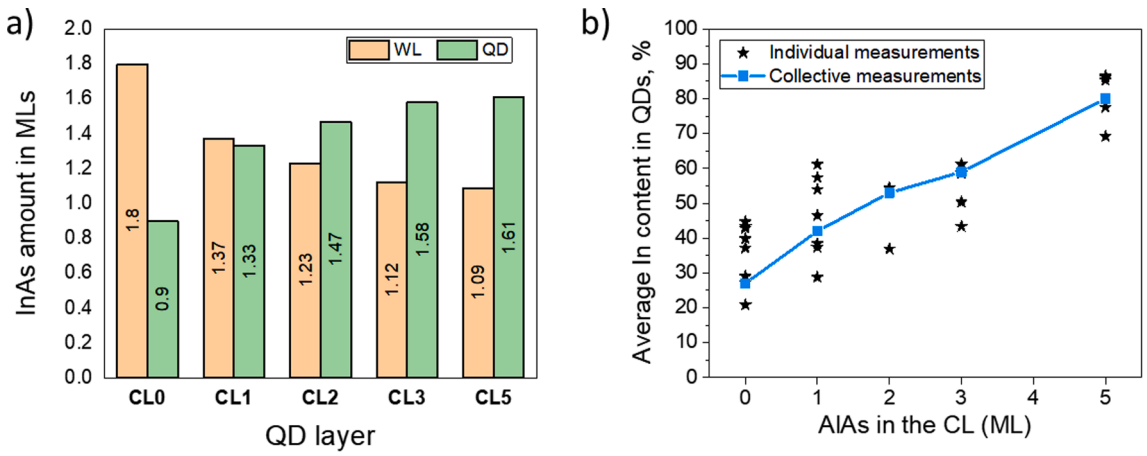

Fig. 5. (a) Vertical stacked bar graph showing the distribution of InAs between the QDs and the WL at different AlAs CL thicknesses. (b) Average In content of individual QDs (black stars) and the one obtained by the statistical model (blue line) for the different layers.

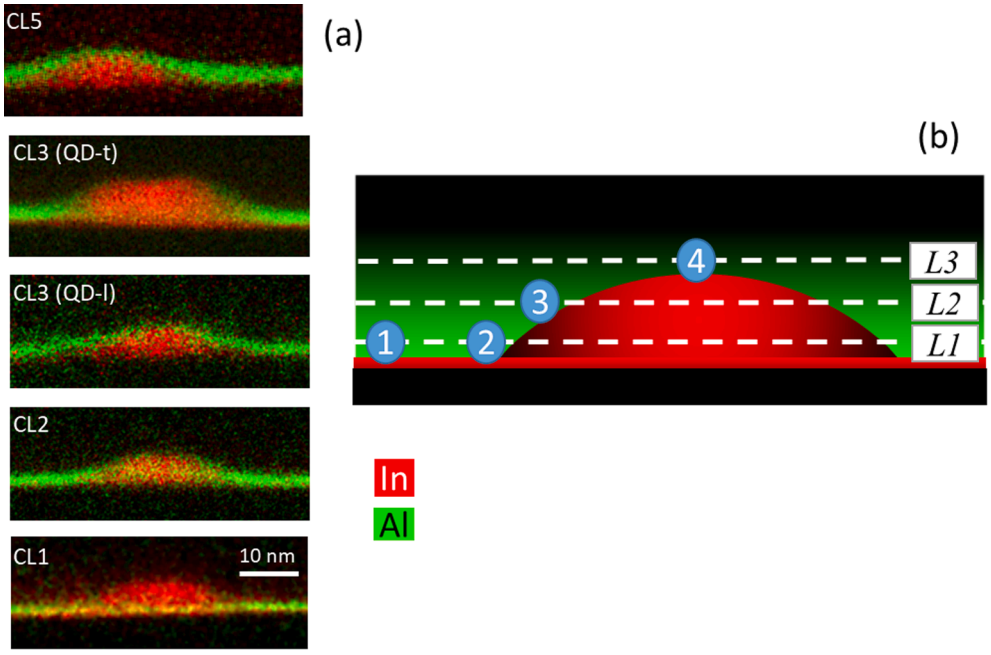

Fig. 6. (a) In and Al compositional EDX maps of QDs from layers up to 5 MLs of AlAs. For the case of **CL3**, we have chosen a giant truncated pyramid (QD-t) and a small lenticular QD (QD-l). (b) Scheme of a QD region with the selected positions for the measurement of Al content, from a position away of the QD (1), at the edge (2), in the middle (3) and above the QD (4). For this, 3 horizontal profiles were carried out, named from L1 at the base to L3 above the QD.

comparing two different capping strategies to protect the integrity of InAs/GaAs QD such as the control of CL growth rate of CL and the use of GaAsSb CLs [28]. It appears that both approaches lead to an increase of the average QD volume by preserving the larger QDs at the expense of the smaller ones, resulting in a reduction of QD density. To check the hypothesis in the AlAs/InAs QD system, QD densities were determined for each layer by means of the simultaneous recording of LAADF images and EELS maps in several regions, which permit to measure the number of QDs and the sample thickness, respectively (using log-ratio method [37,38]). The outcomes are displayed in Fig. 4 together with the average QD volume. As it can be observed, it seems that the AlAs capping obeys the previous rule where the QD density follows an opposite behaviour regarding the average volume. Remarkably, the trend presents a turning point at **CL2**, indicating a variation of mechanism at CL thicknesses around 2–3 MLs of AlAs.

3.2. *Measurement of the average composition of QDs*

In the previous section, we studied how an increase in the thickness of the CL affects the size and density of the QD population in an opposite way. However, that means an uncertainty about the tendency of the average composition of the QDs for each layer since many possibilities fulfil the scenario. To clarify this issue, two procedures have been carried out in order to measure the average In content within the QDs. In the first, we are going to measure the In contents in a collective way making use of density and mean volume measurements, where the overall amount of InAs in the QDs needs to be known [39]. As the total amount of InAs deposited (2.8 ML) must be distributed between the QDs and the WL, the measurement of the In amount in the more homogenous WL allows determining that value. For this, the use of the area under average In profiles along the growth direction of wide WL regions in calibrated layers has been probed as the suitable procedure for this task [26]. Following this calibration, the amounts of InAs in the different WLs

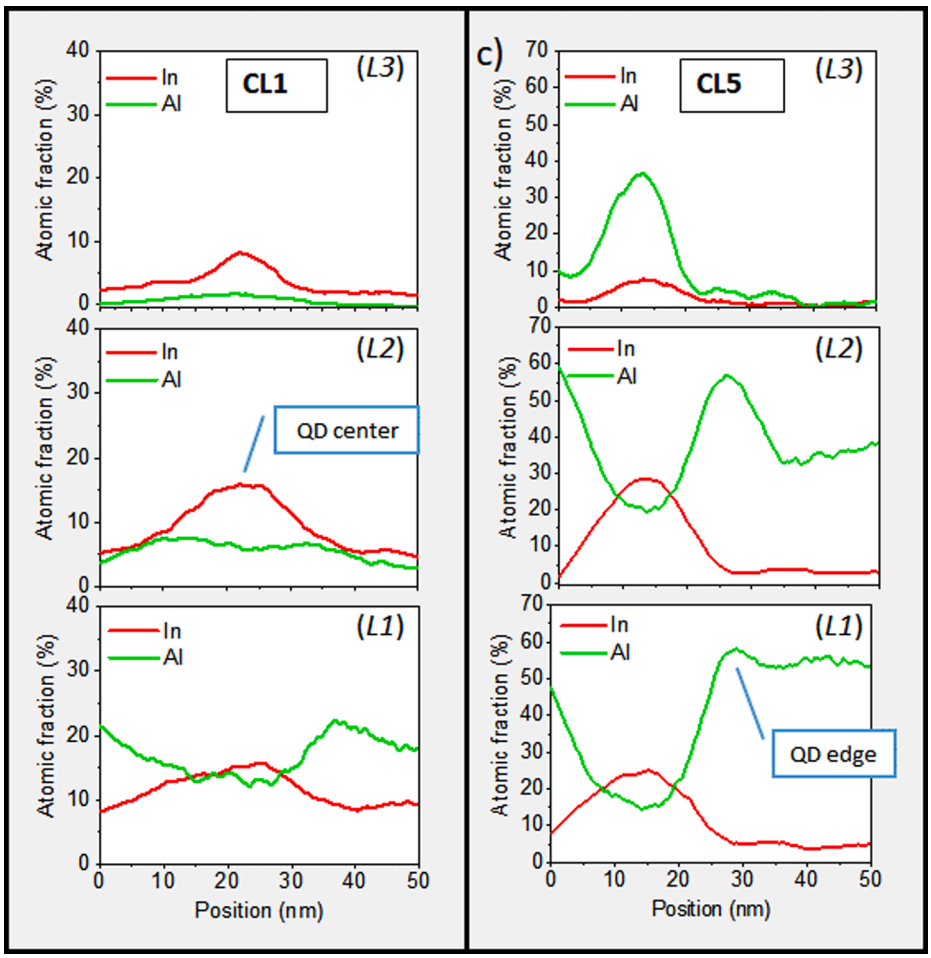

Fig. 7. Parallel profiles to the layer for In and Al contents from high magnification EDX maps for **CL1** and **CL5** QD layers.

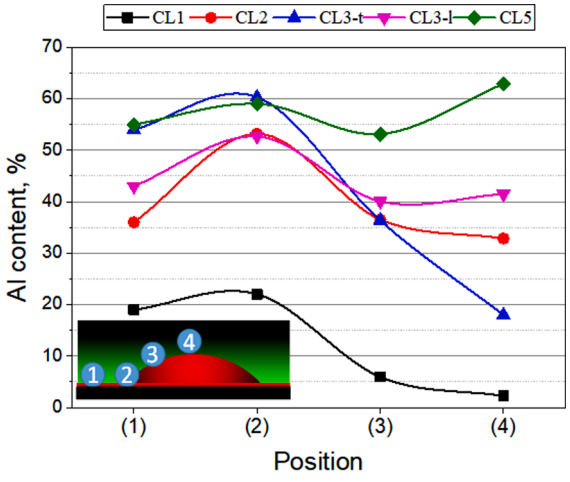

Fig. 8. Al contents of the CL calculated after applying the procedure described in Appendix A for the 4 positions marked in inset: (1) in the WL away the QD, (2) at the QD edge, (3) in the QD middle and (4) over the QD.

expressed as ML of InAs are showed in Fig. 5.a. Certainly, deposition of thicker AlAs capping layers induces to an exponential impoverishment of In of the WL regions, from 1.8 MLs in the layer **CL0** to 1.09 MLs in layer **CL5** [14]. The difference regarding the initial InAs deposition (2.8 ML) corresponds to the amount confined in the QDs considered as a whole. The amount of InAs retained in the QDs after capping almost doubled, from a 33% of the total InAs deposited in the layer **CL0** (0.9 ML of InAs) to a 60% in the layer **CL5** (1.61 MLs of InAs). Now, the average composition of the QDs as a collective can be estimated by using the average volume and density data of the QDs population [26,39]. Fig. 5.b shows these outcomes as a blue line, where a linear increase of In content with the AlAs thickness is appreciated. Certainly, there is an enhancement of the QD protection against decomposition as the thickness of the AlAs layer increases in relation to the GaAs capping. The evolution of average In content versus CL thickness is closely related to QD height, but not to QD density and volume.

To confirm these results, the second procedure tries to estimate the In content from EDX maps of individual QDs taking into account both the QD size and shape together with the TEM sample thickness obtained by EELS. The results for several QDs are shown as black stars in Fig. 5.b. As it can be seen, they exhibit a remarkable dispersion due to several factors, such as the variability of the QDs in each population itself, the error of the methodology and the possibility that the QD may be partially sectioned in the TEM sample preparation. However, there is a very good correspondence between the results obtained from collective and individual measurements. Both indicate that the coverage by thin layers of AlAs has a shielding effect against QD decomposition resulting in bigger and In-richer QDs. Indeed, there is a direct correspondence between the reduction of the WL and the enrichment of the QDs. Covering InAs QD by thin layers of AlAs leads to an important decrease of the WL, not through a substitution of In by Al atoms, as proposed by some authors [12,15,16,20] but by limiting the subsequent lateral back segregation from the eroded QD during capping [36,40,41]. Rather, it seems that deposition of AlAs layers prevents In mobility from QDs to the WL.

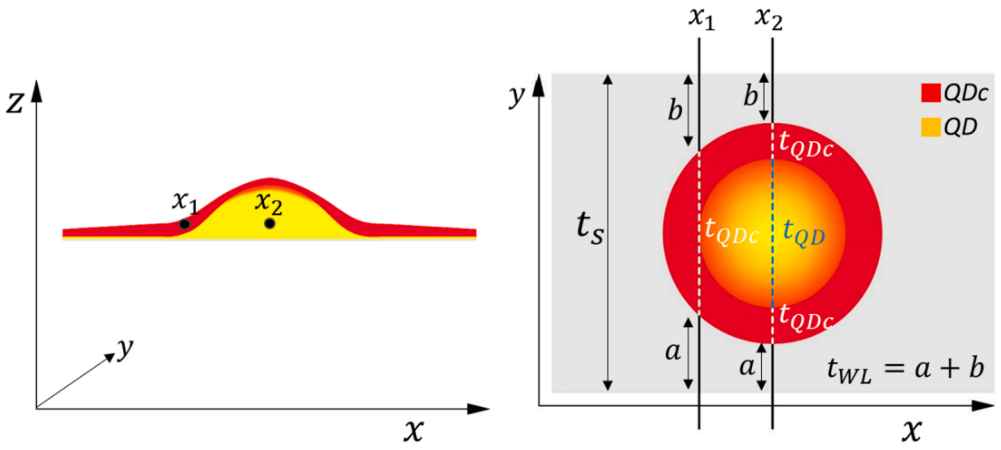

Fig. 9. Illustration of cross-sectional (on the left) and planar view (on the right) images of InAs QD covered with an AlAs layer. Image on the right represent a horizontal section of the QD on the left. The vertical lines show positions crossing the InAs QD by the tangent of QD (x_1) and through the centre (x_2) where the part of white dashed line corresponds to thicknesses of quantum dot coverage, the blue dashed line to the quantum dot and the black line to the GaAs capping layer.

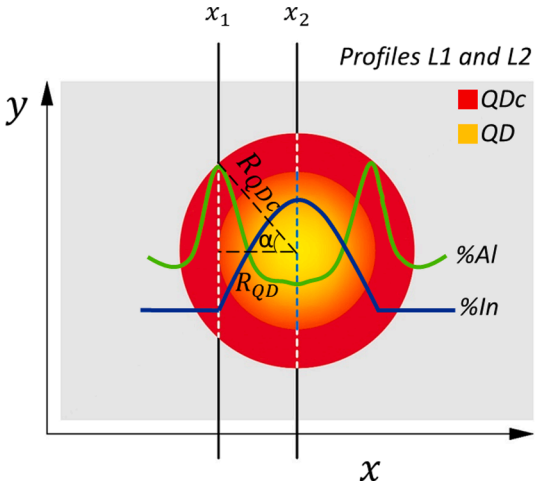

Fig. 10. Theoretical profiles L1 and L2 of the Al and In contents (blue and green lines, respectively) together to the corresponding slice of the AlAs/InAs QD in planar view.

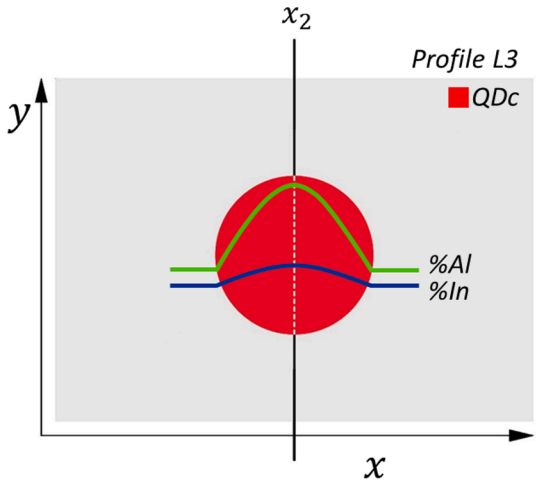

Fig. 11. Planar sectional view of an illustration of InAs QD covered with AlAs together with the In and Al theoretical profiles (blue and green lines, respectively) taken perpendicular to the growth direction. The vertical line shows the position (x_2) that crosses the centre of the QD used to calculate Al values over the QDs.

3.3. Analysis of Al distribution around the QD

As seen above, the increase of AlAs CL thickness gives rise to changes in QDs structure such as size, shape, composition, etc., which not always follows a linear tendency. Likely, it could be related to variations of the Al content and thickness of the CL around the QD that will define the height and width of the potential barrier, and, consequently, the degree of electronic confinement of the QDs. In order to shed new light on these issues, this block is devoted to describe the evolution of the Al distribution in the QD surroundings. Fig. 6.a shows high magnification EDX compositional maps for representative QDs for each QD layer, where green and red channels correspond to Al and In contents, respectively. Although the vast majority of QDs in the considered layers are lenticular, an increasing proportion of QDs with truncated pyramid shape is observed as the CL thickness increases, from 5% in the **CL3** layer to 20% in the **CL5** layer. As the apparition of pyramidal truncated QDs starts in the layer **CL3**, both types of QDs have been studied in this layer: giant truncated QD **(QD-t)** and regular lenticular QD **(QD-l)**. From these images, QDs with thinner layers of AlAs (**CL1**, **CL2** and **CL3 (QD-t)**) seem to be not covered by a defined AlAs layer while this is clearly the case for thicker CLs (**CL3 (QD-l)** and **CL5**). However, special care must be taken with its interpretation because the use of Look-Up Table (LUT) scale images can hide in many times important features from our perception, especially in images with several channels. In addition, the interpretation of EDX mapping is less obvious if different materials are present along the electron beam path, as is the case for quantum dot specimens.

Although the direct interpretation of In and Al maps gives some insight about the presence of Al above the dot, the knowledge of degree of coverage around the islands in terms of thickness and real contents is not straightforward. In other words, there is no information on whether the CL at the top and sides of the QD has the same thickness and composition as in regions between QDs, covering them as a blanket with uniform thickness and content, or, if on the contrary, accumulations or depletions occur in some regions surrounding the QD.

In order to investigate how AlAs is distributed around dots, different compositional profiles parallel to the growth plane are performed for each QD layer, passing through the QD base (*L1*), in the QD middle (*L2*) and to above of the QD (*L3*) (see dashed lines in Fig. 6.b). Thus, Fig. 7 shows Al and In horizontal compositional profiles for the QD in **CL1** (left column) and **CL5** (right column) layers of the Fig. 6, taken along *L1*, *L2* and *L3* directions. The horizontal profiles of the other samples are not showed here and they have intermediate characteristics between these cases. The profiles of QD layer **CL5** clearly present higher In and Al

contents in all regions regarding to those ones in the **CL1** layer. On the one hand, In profiles always show a single maximum that increases from base *(L1)* to the middle (*L2*) and decrease in the region over the QD *(L3)*. The peak amplitudes are narrowed when comparing the *L1* profiles with respect *L2* profiles, which is reasonable for this dot geometry. On the other hand, Al profiles outline a symmetrical configuration consisting of a valley surrounded by two peaks for positions *L1* and *L2*, which decreases as it ascends to the top, forming a single one over the QD in position *L3*. The central valley in *L1* and *L2* corresponds to the centre of the QD and the peaks to the slopes of the QDs. This effect is commonly observed in core-shell nanowires [42]. Moreover, the Al content in the WL regions farthest from the QD reaches a maximum at position *L1* that decays exponentially to zero at position *L3*. From the observation of the In and Al profiles, two important conclusions can be drawn. First, the Al amount over the QD raises with the increase of the CL thickness though the deposition of 1 ML of AlAs barely coats the QD even for the bottom positions. Therefore, the Al content in the QD of **CL1** reaches a maximum content of 18% in the regions between dots while at the top of the QD is 2.5%, almost within the experimental error of the technique. In the case of the QD in layer **CL5**, the CL clearly covers the QD with an Al content of 37% at the apex, however, lower than that measured in the WL regions (58%). Second, the peaks in the *L1* profiles show an Al content greater than of the maximum of the WL region pointing to an accumulation of Al on the first ramps of the edges of the QD.

Either way, the results obtained in EDX profiles have showed the average values of Al throughout the whole TEM sample thickness. In order to obtain a precise picture of the capping structure, it is necessary to determine the actual contents in the small portion where the CL covers the QD. For this, 4 positions are selected for the evaluation of the Al content of the CL, from a position away of the QD (1), at the QD edge (2), in the QD middle (3) and above the QD (4) (Fig. 6.b**)**. The procedures to estimate the Al contents in the CL in these positions around the QD are detailed in the Appendix A. Following the procedures, Fig. 8 presents the estimations of the maximum Al contents for all the QD layers in these 4 positions. It should be noted that results for the positions (2) and (3) measured in the centre and in the tangent to the QD (see Appendix A) are very similar, which verifies the absence of Al within the InAs QD as was originally supposed in the calculus. In general, results for all the regions revealed an increase of Al content covering the QD with increasing CL thickness, but far away from the nominal AlAs design. Comparing the results between the QD layers, several remarkably findings can be derived. First, Al content values of the CL in regions between the dots (WL) are always lower to those in the QD edges. During the AlAs capping, an accumulation in the QD flanks occurs at the beginning of the deposition at least up to 5 ML of AlAs CL. Second, AlAs contents covering the QD apex are similar that those of the WL regions from the deposition of 2 ML onwards, although in the case of giant QD as **QD-t** in the layer **CL3**, the apex covering is not achieved. From our results, it seems that only the QDs with 5 ML of AlAs shows an almost homogeneous coverage, i.e. the CL of AlAs has the smallest differences in Al content between the different measured positions. The AlAs CL works as a blanket without irregularities from this CL thickness.

In addition, EDX mappings evidence the presence of In above the apex for all the QDs in the different layers. Following the same procedure, the In content above the apex (position (4)) were also calculated giving similar values for all the layers (15–20% of In) almost independently of the Al content. The CL on top of the QD is a complex quaternary alloy made of $In_xAl_yGa_{1-x-y}As$ where the In content is almost constant and Al content increases at the expense of Ga.

4. Discussion

Certainly, growth conditions such as temperature, interruptions and/or flux ratios play a key role in the QD formation and in their subsequent changes during the capping [24,43]. Our growth conditions are very similar to others reported in the bibliography. In general, the growers use the same growth temperature for the InAs layer and the AlAs CL. Thus, Kondratenko [44], Löbl [13], Kim [45] and Zhang [46] grow the AlAs/InAs QDs in a Stranski–Krastanov mode at a substrate temperature of ~500 °C, while Varghese [16] used 520 °C or Nevedomskiy [43] 460 °C. Others slightly change the growth conditions of InAs and AlAs, such as Dorogan [23] (520 °C and 480 °C) or ourselves (460 °C and 480 °C), respectively. These are the standard growth conditions that we have always used to obtain the desired QD density and morphology in our MBE equipment. The growth temperature of the CL is only slightly lower than some used by other studies, and slightly higher than in others, so we believe that it should not introduce significant differences in the behavior of In and Al species during capping compared to other studies. Once the QDs are covered by this low-temperature grown layer (1–5 ML of AlAs plus 30 ML of GaAs, all grown at 480 °C) with thicknesses ranging from 7 to 10 nm, the subsequent growth of the GaAs spacer layer at 580 °C should not have a significant effect. At that point, the QDs are fully buried, quite stable and the bulk diffusion is extremely small. In the case of InAs QDs, the annealing temperatures to achieve significant compositional changes in buried nanostructures have to be above 650 °C, as demonstrated in many studies in the literature where ex-situ annealing is performed [23] as well as in the authors' studies on similar structures [47].

In any case, Al atoms cannot boast of large surface displacements once they are adsorbed on the surface at this temperature so should be expected a high degree of QD coverage from the early stages of CL growth. This is consistent with the higher energy barriers for surface diffusion for Al (0.8 eV) [48] as compared to Ga (0.62 eV) [49] or In (0.4 eV) [50]. The surface diffusion lengths at this growth temperature are about few nanometres, dozens of nm or hundreds of nm for Al, Ga and In, respectively. In atoms are highly mobile while Al atoms are almost motionless, remaining very close to the first surface adsorption place. However, the presence of Al at the apex of the QDs is barely detected for the **CL1** layer, although it shows a remarkable rise with the increase of CL thickness (see Fig. 8). Therefore, the WL and QDs are not covered by the AlAs as a blanket with similar thickness and composition for everyone. In the **CL1** layer, the Al content over the QD apex is lower than in the WL regions but it presents similar contents from 2 MLs onwards. As most of the CLs used in the bibliography are in this range, the choice of a CL thickness of 2 ML of AlAs [15,16,44,45] or lower [12,13,51] implies considerable differences in the band structure around the QD. This is also connected to the important accumulation of Al in the initial flanks of the QDs at the beginning. Although surface diffusion is low, Al atoms can be segregated from the apex to the edges of the QDs due to better reticular matching reducing the surface tension energy [21]. Consequently, an accumulation of Al at the edges of the QD initially occurs at the expense of the Al deposited at the apex.

Thus, the decrease of the QD diameter and volume from **CL0** up to **CL3** observed in Fig. 3 could be explained by this accumulation of Al at the QD edges. Therefore, accretion of Al at the QD flanks would hinder the lateral intermixing in the QDs resulting in a smaller expansion of the base diameter during capping. Remarkably, the aspect ratio increases despite of this base reduction as the QD height has an ascending tendency (Fig. 3.b). At any case, a steep decrease in the ground-state energy is expected since the decrease in confinement energy due to increase in height is much larger than the increase in confinement energy due to decrease in base length for this aspect ratio range ($r < 0.4$) [29]. Both the initial reduction of the QD bases and the increase of the aspect ratio are contrary to those results observed in the case of other alloys used as CLs, such as GaAsN or GaAsSb. In general, high resilience against QD decomposition always results in taller, but in turn wider QDs in which the aspect ratio undergoes only small variations [28,52]. This is probably because these anions accumulate preferentially on the apexes rather than on the flanks, leaving these regions of the QDs freer to expand. Thus, the protection against desorption at the peaks (greater height) of these CLs is compensated by a greater degree of intermixing at the QD flanks, which causes a widening of the QD diameter [27]. It

remains to be said that probably the change of trend of the QD bases from 3 ML of AlAs is apparent, since it is due to the widening of the distribution of QD population that begins to occur from that CL thickness. Certainly, a persistence of large dots coexisting with much smaller ones is perceived, raising the mean value.

Since the surface segregation coefficients of In atoms through GaAs or AlAs layers are very similar [18,19], the differences in QD decomposition of these layers are probably due to the desorption of In from the apex before the QDs are capped. At the beginning of the capping process, the InAs areas with bare surface (mainly the top of the QDs) will start to drop indium. On the one hand, as the mobility of Ga atoms is higher than Al, it directly leads to a poor coating when the CL is made of GaAs due to a high lattice mismatch regarding the relaxed InAs apex. On the other hand, the almost immobile Al atoms quickly cover the surface of the QD, freezing the surface redistribution of In, and restraining the loss of In from the QDs during overgrowth. The taller and In-richer QDs observed as the CL thickness increases may be explained by a progressive hindering effect of Al atoms in the surface migration of In.

Certainly, AlAs CL evidences a strong shield effect against QD decomposition. The average QD height in the **CL5** layer raises about 28% compared to the **CL0** layer. This value is generally higher that the obtained by applying other protection strategies such as increasing the GaAs growth rate [53] or using different GaAs(Sb)(N) CLs [27,54]. Moreover, although CLs with better levels of protection have been reported, such as with $In_{0.08}Ga_{0.92}As_{0.96}N_{0.04}$ [54] or $GaAs_{0.75}Sb_{0.25}$ [55], these layers tend to have secondary drawbacks. On the one hand, the incorporation of layers with high Sb contents produces a high increase in residual stresses, which can lead to the appearance of defects in the case of MQWs, while Al(Ga)As is almost lattice matched with GaAs. On the other hand, the incorporation of N easily generates punctual defects that ultimately lead to a reduction of the carrier diffusion length and an increase of the background doping [56,57].

However, an excess of protection against QD erosion by using thicker AlAs has detrimental effects since it practically freezes the initial population of QDs before capping, which is quite heterogeneous. Certainly, TEM measurements of uncapped QDs have revealed that there are about 5–10% of giant QDs, probably due to a coalescing effect [52,58,59]. During normal GaAs capping there is a homogenization of QD sizes, where the presence of such giants QDs in the buried layers is almost null. These giant QDs are strongly eroded during GaAs capping resulting in many cases in ring structures [60]. In the case of using thick AlAs CLs, the uncapped QDs do not undergo this levelling effect and this explains the wide dispersion of sizes observed in the histograms of Fig. 2, with the presence of such QD giants. The absence of a certain QD size levelling and the persistence of giant QDs are great handicaps for MQD structures, such as those used in QDSC and photodetectors. The spacers thickness between QD layers should be chosen large enough to minimize defects formation and suppress tunnelling between QDs (greater than 5–10 nm), but not too much, since spacer layers with a thickness greater than 30 nm limit the efficiency, suppress the electrons transfer between QDs and facilitate the accumulation of charge in the QD [16]. The persistence of such giant QDs with heights of more than 10 nm exacerbates the accumulation of stresses in the subsequent layers leading to the formation of dislocations and agglomerations [61] as sometimes we have been observed in the upper layers. This fact would explain why almost all successful studies in the capping of InAs MQDs by AlAs layers use very thin thicknesses (<5 ML).

5. Conclusions

In summary, the use of different CL thicknesses made of AlAs not only modifies the shape, aspect ratio and composition of the InAs QDs but also of the Al distribution over them. First, the size distributions of the QD population are gradually split for CL thickness above 5 ML in a bimodal distribution where lenticular shape QDs coexist with huge truncated pyramids. Based on this heterogeneity, thicknesses above 5 ML must be discarded in the design of MQD structures when using AlAs CLs. Second, the QD heights and average InAs QD contents increase progressively as the CL thickness rises demonstrating that AlAs coverage has a high shielding effect against QD decomposition. Nevertheless, an excess of protection of AlAs against QD erosion could have harmful effects since giant QDs can survive. Remarkably, QD base diameters experience a decay for shorter CL thicknesses leading to an aspect ratio increase. Third, Al contents around the QDs increase with the CL thickness but it is far away from the nominal AlAs design. In addition, its distribution is non-uniform tending to accumulate at the QD flanks at the expense of Al deposited at the apex. Al contents above the QD apex are similar to those of the WL from 2 ML thick, but it only behaves as a continuous blanket without irregularities from 5 ML onwards. CL features such as the degree of coverage, Al real contents, accumulation at the edges and/or the presence of In in the CL over the QDs must be considered when performing theoretical models in QD device level simulations

CRediT authorship contribution statement

N. Ruiz-Marín: Writing – original draft, Writing – review & editing, Investigation, Formal analysis. **D.F. Reyes:** Data curation, Writing – review & editing. **L. Stanojević:** Investigation. **T. Ben Investigatio:** Project administration. **V. Braza:** . **A. Gallego-Carro:** Investigation. **G. Bárcena-González:** Investigation. **J.M. Ulloa:** Conceptualization, Project administration. **D. González:** Supervision, Methodology, Writing – review & editing, Project administration.

Declaration of Competing Interest

The authors declare that they have no known competing financial interests or personal relationships that could have appeared to influence the work reported in this paper.

Acknowledgements

The work has been co-financed by the Spanish National Research Agency (AEI projects MAT2016-77491-C2-2-R and PID2019-106088RB-C33), Regional Government of Andalusia (project FEDER-UCA18-108319) and the European Regional Development Fund (ERDF).

Appendix A

Estimation of real contents in the AlAs CL around the QD

In order to interpret correctly the results and calculate the real contents of the CL around the QD it is necessary to take into account both the sample thickness and the geometry of the objects. To address this need, TEM sample thickness maps were taken by means of low-loss EELS using the ratio between zero-loss electrons and the total transmitted intensity (log-ratio method) in the spectra. Fig. 9 shows a scheme of a slice of an InAs QD covered with AlAs capping in cross-sectional (on the left) and planar view (on the right) where the InAs QD is coloured in yellow, the AlAs coverage in red and the GaAs spacer layer in grey. As the geometry of the vast majority of buried dots adopted lenticular shape, a circular geometry was assumed for QDs. The contributions of the regions away the QD, inside the QD and over the QD will be denoted with subscripts *WL*, *QD*, *QDc*, respectively. Two vertical

lines crossing the InAs QD are defined, at the tangent of QD (x_1) and by the centre (x_2), where $t_s$is the sample thickness, t_{WL} is the sum of the thicknesses of the regions out the QDs, t_{QD} is the InAs quantum dot diameter (chord of circumference *QD*), and t_{QDc} is the AlAs CL thickness just around the QD (chord of circumference *QDc*). Henceforth, note that these parameters lengths vary depending on the position (x_1, x_2) and the profile considered.

According to this, AlAs contents can be estimated in any region knowing the experimental Al content measured through EDX measurements, $\%Al_x^{EDX}$, as follows:

$$\%\mathrm{Al}_x^{\mathrm{EDX}}\mathrm{t}_s = \%\mathrm{Al}_{\mathrm{QDc}}\ \mathrm{t}_{\mathrm{QDc}} + \%\mathrm{Al}_{\mathrm{QD}}\ \mathrm{t}_{\mathrm{QD}} + \%\mathrm{Al}_{\mathrm{WL}}\ \mathrm{t}_{\mathrm{WL}} \tag{A.1}$$

where $\%Al$ is the average Al content for each of the zones mentioned above. To compute the real maximum Al contents in the 4 positions of our special interest, we have extracted horizontal profiles *L1, L2,* and *L3* (as described in the scheme of Fig. 6**)** and measured the horizontal dimensions of each object.

Real Al contents at the QD flanks from profiles L1 and L2

Fig. 10 shows the horizontal profiles of Al and In together to a planar view representation of a slice of the system where R_{QDc} and R_{QD} are the radii of the AlAs coverage + QD and the QD, respectively. In order to estimate the Al content in the QD flanks two positions were selected for comparison: x_1, tangent to the InAs QD and x_2, which passes through the centre of the QD.

For the first position, x_1 the equation (A1) can be simplified as follows since the term concerning InAs QD is null:

$$\%Al_{x_1}^{EDX} t_{s_{x1}} = \%Al_{QDc} t_{QDc} + \%Al_{WL} t_{WL} \tag{A.2}$$

where

$$t_{WL} = t_{s_{x1}} - t_{QDc} \tag{A.3}$$

and

$$t_{QDc} = 2\sin\alpha R_{QDc} \tag{A.4}$$

where α is the angle between R_{QD} and R_{QDc} as defined in Fig. 10. Thus, this equation can be written as:

$$t_{QDc} = 2\sin(\cos^{-1}(\frac{R_{QD}}{R_{QDc}}))R_{QDc} \tag{A.5}$$

Finally, replacing the equations (A.3) and (A.5) in (A.2) and rearranging it, the real Al content on the QDs edges can be obtained as:

$$\%Al_{QDc}^{edge}(x_1) = \frac{(\%Al_{x_1}^{EDX} t_{s_{x1}}) - \%Al_{WL}(t_{s_{x1}} - t_{QDc})}{2\sin(\cos^{-1}(\frac{R_{QD}}{RQDc}))R_{QDc}} \tag{A.6}$$

For the second position, x_2, $R_{QDc} = t_{QDc} + t_{QD}$ and the thicknesses t_{WL} and t_{QDc} are given respectively by:

$$t_{WL} = t_{s_{x2}} - t_{QDc} - t_{QD} = t_{s_{x2}} - 2R_{QDc} \tag{A.7}$$

$$t_{QDc} = 2(R_{QDc} - R_{QD}) \tag{A.8}$$

Using the Al content data measured in the QD centre, $\%Al_{x_2}^{EDX}$, the real content on the QDs edges in position x_2 can be calculated substituting the equations (A.7) and (A.8) in (A.2) according to:

$$\%Al_{QDc}^{edge}(x_2) = \frac{(\%Al_{x_2}^{EDX} t_{s_{x2}}) - \%Al_{WL}(t_{s_{x2}} - 2R_{QDc})}{2(R_{QDc} - R_{QD})} \tag{A.9}$$

Real Al content over the QD apex in profile L3

Fig. 11 shows the corresponding slice in planar view with the Al and In theoretical profiles where only the position x_2, is of interest. As the horizontal profile *L3* is out of the QD, t_{QD} is null and Eq. (A.1) can be simplified by eliminating the term corresponding to the InAs QD. In this region, essentially only AlAs coverage contributes (as illustrated in Fig. 5) and the thicknesses t_{WL} and t_{QDc} can be obtained as follows:

$$t_{WL} = t_{s_{x2}} - t_{QDc} \tag{A.10}$$

$$t_{QDc} = 2R_{QDc} \tag{A.11}$$

Then, the Al fraction over the InAs QD can be got replacing the equations (A.10) and (A.11) in (A.2):

$$\%Al_{QDc}^{over}(x_2) = \frac{(\%Al_{x_2}^{EDX} t_{s_{x2}}) - \%Al_{WL}(t_{s_{x2}} - 2R_{QDc})}{2R_{QDc}}$$

References

[1] M.V. Rakhlin, K.G. Belyaev, G.V. Klimko, I.S. Mukhin, D.A. Kirilenko, T.V. Shubina, S.V. Ivanov, A.A. Toropov, InAs/AlGaAs quantum dots for single-photon emission in a red spectral range, Sci. Rep. 8 (1) (2018), https://doi.org/10.1038/s41598-018-23687-7.

[2] D. Rivas, G. Muñoz-Matutano, J. Canet-Ferrer, R. García-Calzada, G. Trevisi, L. Seravalli, P. Frigeri, J.P. Martínez-Pastor, Two-color single-photon emission from InAs quantum dots: Toward logic information management using quantum light, Nano Lett. 14 (2) (2014) 456–463, https://doi.org/10.1021/nl403364h.

[3] D. Cogan, O. Kenneth, N.H. Lindner, G. Peniakov, C. Hopfmann, D. Dalacu, P. J. Poole, P. Hawrylak, D. Gershoni, Depolarization of Electronic Spin Qubits Confined in Semiconductor Quantum Dots, Phys. Rev. X. 8 (2018), 041050, https://doi.org/10.1103/PhysRevX.8.041050.

[4] P. Holewa, M. Gawełczyk, A. Maryński, P. Wyborski, J.P. Reithmaier, G. Sęk, M. Benyoucef, M. Syperek, Optical and Electronic Properties of Symmetric InAs/(In, Al, Ga)As/In P Quantum Dots Formed by Ripening in Molecular Beam Epitaxy: A Potential System for Broad-Range Single-Photon Telecom Emitters, Phys. Rev. Appl. 14 (2020), https://doi.org/10.1103/PhysRevApplied.14.064054.

[5] Y.-J. Ma, Y.-G. Zhang, Y.i. Gu, X.-Y. Chen, P. Wang, B.-C. Juang, A. Farrell, B.-L. Liang, D.L. Huffaker, Y.-H. Shi, W.-Y. Ji, B. Du, S.-P. Xi, H.-J. Tang, J.-X. Fang, Enhanced Carrier Multiplication in InAs Quantum Dots for Bulk Avalanche Photodetector Applications, Adv. Opt. Mater. 5 (9) (2017) 1601023, https://doi.org/10.1002/adom.v5.910.1002/adom.201601023.

[6] Z.H. Chen, O. Baklenov, E.T. Kim, I. Mukhametzhanov, J. Tie, A. Madhukar, Z. Ye, J.C. Campbell, InAs/AlxGa1-xAs quantum dot infrared photodetectors with undoped active region, Infrared Phys. Technol. 42 (3-5) (2001) 479–484, https://doi.org/10.1016/S1350-4495(01)00109-8.

[7] A.J. Nozik, Quantum dot solar cells, Phys. E Low-Dimensional Syst. Nanostructures. 14 (1-2) (2002) 115–120, https://doi.org/10.1016/S1386-9477(02)00374-0.

[8] K.A. Sablon, J.W. Little, V. Mitin, A. Sergeev, N. Vagidov, K. Reinhardt, Strong enhancement of solar cell efficiency due to quantum dots with built-in charge, Nano Lett. 11 (6) (2011) 2311–2317, https://doi.org/10.1021/nl200543v.

[9] N.S. Beattie, P. See, G. Zoppi, P.M. Ushasree, M. Duchamp, I. Farrer, D.A. Ritchie, S. Tomić, Quantum Engineering of InAs/GaAs Quantum Dot Based Intermediate Band Solar Cells, ACS Photonics. 4 (11) (2017) 2745–2750, https://doi.org/10.1021/acsphotonics.7b0067310.1021/acsphotonics.7b00673.s001.

[10] M. Zieliński, Vanishing fine structure splitting in highly asymmetric InAs/InP quantum dots without wetting layer, Sci. Rep. 10 (2020) 1–13, https://doi.org/10.1038/s41598-020-70156-1.

[11] F. Cappelluti, A. Khalili, M. Gioannini, Open circuit voltage recovery in quantum dot solar cells: A numerical study on the impact of wetting layer and doping, IET Optoelectron. 11 (2) (2017) 44–48, https://doi.org/10.1049/ote2.v11.210.1049/iet-opt.2016.0069.

[12] X.M. Lu, S. Matsubara, Y. Nakagawa, T. Kitada, T. Isu, Suppression of photoluminescence from wetting layer of InAs quantum dots grown on (311)B GaAs with AlAs cap, J. Cryst. Growth. 425 (2015) 106–109, https://doi.org/10.1016/j.jcrysgro.2015.02.074.

[13] M.C. Löbl, S. Scholz, I. Söllner, J. Ritzmann, T. Denneulin, A. Kovács, B. E. Kardynał, A.D. Wieck, A. Ludwig, R.J. Warburton, Excitons in InGaAs Quantum Dots without Electron Wetting Layer States, Commun. Phys. 2 (2019) 1–7. https://academic.microsoft.com/paper/2967909350.

[14] N. Ruiz-Marín, D.F. Reyes, L. Stanojević, T. Ben, A. Gallego-Carro, E. Luna, J.M. Ulloa, D. González, Suppressing the Wetting Layer effect after AlAs capping in InAs/GaAs quantum dot solar cells, Appl. Surf. Sci. in review (2021).

[15] F.K. Tutu, P. Lam, J. Wu, N. Miyashita, Y. Okada, K.-H. Lee, N.J. Ekins-Daukes, J. Wilson, H. Liu, InAs/GaAs quantum dot solar cell with an AlAs cap layer, Appl. Phys. Lett. 102 (16) (2013) 163907, https://doi.org/10.1063/1.4803459.

[16] A. Varghese, M. Yakimov, V. Tokranov, V. Mitin, K. Sablon, A. Sergeev, S. Oktyabrsky, Complete voltage recovery in quantum dot solar cells due to suppression of electron capture, Nanoscale. 8 (13) (2016) 7248–7256, https://doi.org/10.1039/C5NR07774E.

[17] M. Arzberger, U. Käsberger, G. Böhm, G. Abstreiter, Influence of a thin AlAs cap layer on optical properties of self-assembled InAs/GaAs quantum dots, Appl. Phys. Lett. 75 (25) (1999) 3968–3970, https://doi.org/10.1063/1.125509.

[18] S. Oktyabrsky, V. Tokranov, G. Agnello, J. Van Eisden, M. Yakimov, Nano-engineering approaches to self-assembled InAs quantum dot laser medium, J. Electron. Mater. 35 (5) (2006) 822–833, https://doi.org/10.1007/BF02692535.

[19] M. Schowalter, A. Rosenauer, D. Gerthsen, M. Arzberger, M. Bichler, G. Abstreiter, Investigation of In segregation in InAs/AlAs quantum-well structures, Appl. Phys. Lett. 79 (26) (2001) 4426–4428, https://doi.org/10.1063/1.1427148.

[20] A.F. Tsatsul'nikov, A.R. Kovsh, A.E. Zhukov, Y.M. Shernyakov, Y.G. Musikhin, V. M. Ustinov, N.A. Bert, P.S. Kop'ev, Z.I. Alferov, A.M. Mintairov, J.L. Merz, N. N. Ledentsov, D. Bimberg, Volmer-Weber and Stranski-Krastanov InAs-(Al, Ga)As quantum dots emitting at 1.3 μm, J. Appl. Phys. 88 (11) (2000) 6272–6275, https://doi.org/10.1063/1.1321795.

[21] F. Ferdos, S. Wang, Y. Wei, M. Sadeghi, Q. Zhao, A. Larsson, Influence of initial GaAs and AlAs cap layers on InAs quantum dots grown by molecular beam epitaxy, J. Cryst. Growth. 251 (1-4) (2003) 145–149, https://doi.org/10.1016/S0022-0248(02)02471-5.

[22] F. Ferdos, S. Wang, Y. Wei, A. Larsson, M. Sadeghi, Q. Zhao, Influence of a thin GaAs cap layer on structural and optical properties of InAs quantum dots, Appl. Phys. Lett. 81 (7) (2002) 1195–1197, https://doi.org/10.1063/1.1500778.

[23] V.G. Dorogan, Y.I. Mazur, J.H. Lee, Z.M. Wang, M.E. Ware, G.J. Salamo, Thermal peculiarity of AlAs-capped InAs quantum dots in a GaAs matrix, J. Appl. Phys. 104 (10) (2008) 104303, https://doi.org/10.1063/1.3020521.

[24] A. Schramm, J. Schaefer, T. Kipp, C. Heyn, W. Hansen, Shape transformation of self-assembled InAs quantum dots by overgrowth with GaAs and AlAs, J. Cryst. Growth. 301–302 (2007) 748–750, https://doi.org/10.1016/j.jcrysgro.2006.11.157.

[25] F.K. Tutu, I.R. Sellers, M.G. Peinado, C.E. Pastore, S.M. Willis, A.R. Watt, T. Wang, H.Y. Liu, Improved performance of multilayer InAs/GaAs quantum-dot solar cells using a high-growth-temperature GaAs spacer layer, J. Appl. Phys. 111 (2012) 3–6, https://doi.org/10.1063/1.3686184.

[26] D. González, V. Braza, A.D. Utrilla, A. Gonzalo, D.F. Reyes, T. Ben, A. Guzman, A. Hierro, J.M. Ulloa, Quantitative analysis of the interplay between InAs quantum dots and wetting layer during the GaAs capping process, Nanotechnology. 28 (42) (2017) 425702, https://doi.org/10.1088/1361-6528/aa83e2.

[27] D. González, D.F. Reyes, T. Ben, A.D. Utrilla, A. Guzman, A. Hierro, J.M. Ulloa, Influence of Sb/N contents during the capping process on the morphology of InAs/GaAs quantum dots, Sol. Energy Mater. Sol. Cells. 145 (2016) 154–161, https://doi.org/10.1016/j.solmat.2015.07.015.

[28] D. González, S. Flores, N. Ruiz-Marín, D.F. Reyes, L. Stanojević, A.D. Utrilla, A. Gonzalo, A. Gallego Carro, J.M. Ulloa, T. Ben, Evaluation of different capping strategies in the InAs/GaAs QD system: Composition, size and QD density features, Appl. Surf. Sci. 537 (2021) 148062, https://doi.org/10.1016/j.apsusc.2020.148062.

[29] C.Y. Ngo, S.F. Yoon, W.J. Fan, S.J. Chua, Effects of size and shape on electronic states of quantum dots, Phys. Rev. B. 74 (2006), 245331, https://doi.org/10.1103/PhysRevB.74.245331.

[30] M. Califano, P. Harrison, Composition, volume, and aspect ratio dependence of the strain distribution, band lineups and electron effective masses in self-assembled pyramidal In[sub 1–x]Ga[sub x]As/GaAs and Si[sub x]Ge[sub 1–x]/Si quantum dots, J. Appl. Phys. 91 (1) (2002) 389, https://doi.org/10.1063/1.1410318.

[31] W.S. Liu, C.M. Chang, Capping InAs quantum dots with an InGaAsSb strain-reducing layer to improve optical properties and dot-size uniformity, Thin Solid Films. 570 (2014) 490–495, https://doi.org/10.1016/j.tsf.2014.04.032.

[32] Y.H. Chen, J. Sun, P. Jin, Z.G. Wang, Z. Yang, Evolution of wetting layer of InAs/GaAs quantum dots studied by reflectance difference spectroscopy, Appl. Phys. Lett. 88 (7) (2006) 071903, https://doi.org/10.1063/1.2175489.

[33] R.M. Makhijani, N. Halder, S. Sengupta, S. Chakrabarti, Temperature dependent photoluminescence investigation of the effect of growth pause induced ripening in InAs/GaAs quantum dot heterostructures, Mater. Res. Bull. 47 (3) (2012) 820–825, https://doi.org/10.1016/j.materresbull.2011.11.059.

[34] A. Michon, G. Patriarche, G. Beaudoin, G. Saint-Girons, N. Gogneau, I. Sagnes, Density of InAs/InP(001) quantum dots grown by metal-organic vapor phase epitaxy: Independent effects of InAs and cap-layer growth rates, Appl. Phys. Lett. 91 (10) (2007) 102107, https://doi.org/10.1063/1.2779101.

[35] G. Agnello, V. Tokranov, M. Yakimov, M. Lamberti, Y. Zheng, S. Oktyabrsky, Structural and Optical Effects of Capping Layer Material and Growth Rate on the Properties of Self-Assembled InAs Quantum Dot Structures, MRS Proc. 829 (2004) B2.1, https://doi.org/10.1557/PROC-829-B2.1.

[36] G.D. Lian, J. Yuan, L.M. Brown, G.H. Kim, D.A. Ritchie, Modification of InAs quantum dot structure by the growth of the capping layer, Appl. Phys. Lett. 73 (1) (1998) 49–51, https://doi.org/10.1063/1.121719.

[37] H.-R. Zhang, R.F. Egerton, M. Malac, Local thickness measurement through scattering contrast and electron energy-loss spectroscopy, Micron. 43 (1) (2012) 8–15, https://doi.org/10.1016/j.micron.2011.07.003.

[38] T. Malis, S.C. Cheng, R.F. Egerton, EELS log-ratio technique for specimen-thickness measurement in the TEM, J. Electron Microsc. Tech. 8 (2) (1988) 193–200, https://doi.org/10.1002/(ISSN)1553-081710.1002/jemt.v8:210.1002/jemt.1060080206.

[39] P.B. Joyce, T.J. Krzyzewski, G.R. Bell, B.A. Joyce, T.S. Jones, Composition of InAs quantum dots on GaAs(001): Direct evidence for (In, Ga)As alloying, Phys. Rev. B. 58 (24) (1998) R15981–R15984, https://doi.org/10.1103/PhysRevB.58.R15981.

[40] H. Eisele, P.h. Ebert, N. Liu, A.L. Holmes, C.-K. Shih, Reverse mass transport during capping of In 0.5 Ga 0.5 As/GaAs quantum dots, Appl. Phys. Lett. 101 (23) (2012) 233107, https://doi.org/10.1063/1.4769100.

[41] J.M. Ulloa, I.W.D. Drouzas, P.M. Koenraad, D.J. Mowbray, M.J. Steer, H.Y. Liu, M. Hopkinson, Suppression of InAsGaAs quantum dot decomposition by the incorporation of a GaAsSb capping layer, Appl. Phys. Lett. 90 (21) (2007) 213105, https://doi.org/10.1063/1.2741608.

[42] Y. Jung, S.-H. Lee, A.T. Jennings, R. Agarwal, Core-shell heterostructured phase change nanowire multistate memory, Nano Lett. 8 (7) (2008) 2056–2062, https://doi.org/10.1021/nl801482z10.1021/nl801482z.s001.

[43] V.N. Nevedomskiy, N.A. Bert, V.V. Chaldyshev, V.V. Preobrazhenskiy, M. A. Putyato, B.R. Semyagin, Electron microscopy of GaAs-based structures with InAs and As quantum dots separated by an AlAs barrier, Semiconductors. 47 (9) (2013) 1185–1192, https://doi.org/10.1134/S1063782613090170.

[44] S. Kondratenko, O. Kozak, S. Rozouvan, Y.I. Mazur, Y. Maidaniuk, J. Wu, S. Wu, Z. M. Wang, S. Chan, D. Kim, H. Liu, G.J. Salamo, Carrier dynamics and recombination in silicon doped InAs/GaAs quantum dot solar cells with AlAs cap layers, Semicond. Sci. Technol. 35 (11) (2020) 115018, https://doi.org/10.1088/1361-6641/abb1c7.

[45] D. Kim, M. Tang, J. Wu, S. Hatch, Y. Maidaniuk, V. Dorogan, Y.I. Mazur, G. J. Salamo, H. Liu, A. Fernandez, Si-Doped InAs/GaAs Quantum Dot Solar Cell with AlAs Cap Layers, E3S Web Conf. 16 (2017) 16001, https://doi.org/10.1051/e3sconf/20171616001.

[46] Z. Zhang, S. Tan, Y. Kim, Z. Liu, P.J. Reece, S.P. Bremner, Effect of Sb and As spray on emission characteristics of InAs quantum dots with AlAs capping layer, J. Phys.

D. Appl. Phys. 50 (40) (2017) 405104, https://doi.org/10.1088/1361-6463/aa8660.
[47] J.M. Ulloa, J.M. Llorens, B. Alén, D.F. Reyes, D.L. Sales, D. González, A. Hierro, B. Al??n, D.F. Reyes, D.L. Sales, D. Gonz??lez, A. Hierro, High efficient luminescence in type-II GaAsSb-capped InAs quantum dots upon annealing, Appl. Phys. Lett. 101 (2012), 253112, https://doi.org/10.1063/1.4773008.
[48] Makoto Kasu, Naoki Kobayashi, Surface-diffusion and step-bunching mechanisms of metalorganic vapor-phase epitaxy studied by high-vacuum scanning tunneling microscopy, J. Appl. Phys. 78 (5) (1995) 3026–3035, https://doi.org/10.1063/1.360053.
[49] Makoto Kasu, Naoki Kobayashi, Surface diffusion of AlAs on GaAs in metalorganic vapor phase epitaxy studied by high-vacuum scanning tunneling microscopy, Appl. Phys. Lett. 67 (19) (1995) 2842–2844, https://doi.org/10.1063/1.114803.
[50] K. Fujiwara, A. Ishii, T. Aisaka, First principles calculation of Indium migration barrier energy on an InAs(001) surface, Thin Solid Films. 464–465 (2004) 35–37, https://doi.org/10.1016/j.tsf.2004.06.062.
[51] D. Hu, C.C. McPheeters, E.T. Yu, D.M. Schaadt, Improvement of performance of InAs quantum dot solar cell by inserting thin AlAs layers, Nanoscale Res. Lett. 6 (2011) 83, https://doi.org/10.1186/1556-276X-6-83.
[52] D González, D F Reyes, A D Utrilla, T Ben, V Braza, A Guzman, A Hierro, J M Ulloa, General route for the decomposition of InAs quantum dots during the capping process, Nanotechnology. 27 (12) (2016) 125703, https://doi.org/10.1088/0957-4484/27/12/125703.
[53] A.D. Utrilla, D.F. Grossi, D.F. Reyes, A. Gonzalo, V. Braza, T. Ben, D. González, A. Guzman, A. Hierro, P.M. Koenraad, J.M. Ulloa, Size and shape tunability of self-assembled InAs/GaAs nanostructures through the capping rate, Appl. Surf. Sci. 444 (2018) 260–266, https://doi.org/10.1016/j.apsusc.2018.03.098.
[54] J.G. Keizer, J.M. Ulloa, A.D. Utrilla, P.M. Koenraad, InAs quantum dot morphology after capping with In, N, Sb alloyed thin films, Appl. Phys. Lett. 104 (5) (2014) 053116, https://doi.org/10.1063/1.4864159.
[55] J.M. Ulloa, R. Gargallo-Caballero, M. Bozkurt, M. del Moral, A. Guzmán, P. M. Koenraad, A. Hierro, GaAsSb-capped InAs quantum dots: From enlarged quantum dot height to alloy fluctuations, Phys. Rev. B. 81 (2010), 165305, https://doi.org/10.1103/PhysRevB.81.165305.
[56] Ville Polojärvi, Arto Aho, Antti Tukiainen, Andreas Schramm, Mircea Guina, Comparative study of defect levels in GaInNAs, GaNAsSb, and GaInNAsSb for high-efficiency solar cells, Appl. Phys. Lett. 108 (12) (2016) 122104, https://doi.org/10.1063/1.4944844.
[57] A.D. Utrilla Lomas, Tuning the properties of InAs/GaAs quantum dots through a modified capping layer: Application to optoelectronic devices, Universidad Politécnica de Madrid (2017), https://doi.org/10.20868/UPM.thesis.47348.
[58] I. Kamiya, I. Tanaka, H. Sakaki, Control of size and density of self-assembled InAs dots on (001)GaAs and the dot size dependent capping process, J. Cryst. Growth. 201–202 (1999) 1146–1149, https://doi.org/10.1016/S0022-0248(99)00005-6.
[59] Lijuan Wang, Wenwu Pan, Xiren Chen, Xiaoyan Wu, Jun Shao, Shumin Wang, Influence of Bi on morphology and optical properties of InAs QDs: publisher's note, Opt. Mater. Express. 8 (9) (2018) 2702, https://doi.org/10.1364/OME.8.002702.
[60] Daniel Granados, Jorge M García, In(Ga)As self-assembled quantum ring formation by molecular beam epitaxy, Appl. Phys. Lett. 82 (15) (2003) 2401–2403, https://doi.org/10.1063/1.1566799.
[61] N. Ruiz-Marín, D.F. Reyes, V. Braza, S. Flores, A. Gonzalo, J.M. Ulloa, T. Ben, D. González, Formation mechanisms of agglomerations in high-density InAs/GaAs quantum dot multi-layer structures, Appl. Surf. Sci. 508 (2020) 145218, https://doi.org/10.1016/j.apsusc.2019.145218.